ADVANCED OPTICAL MATERIALS
www.advopticalmat.de

The Optical Constants of Solution-Processed Semiconductors—New Challenges with Perovskites and Non-Fullerene Acceptors

Robin Kerremans, Christina Kaiser, Wei Li, Nasim Zarrabi, Paul Meredith, and Ardalan Armin**

Accurate determination of the optical constants of thin film solids has been an ongoing endeavor in optoelectronics and related fields for decades. These constants, namely the refractive index and extinction (or attenuation) coefficient, are the fundamental material properties that dictate electromagnetic field propagation in any medium. They form the inputs to well-established models that allow for design and optimization of multilayer stack structures such as thin film solar cells, light-emitting diodes, and photodetectors. These determinations are particularly challenging for materials that are scattering and highly absorbing. In this work, a new and resource-efficient approach for optical constant determination based upon transmission spectrophotometry in combination with an iterative, reverse transfer matrix model and the Kramers–Kronig relation is reported. The approach is validated using more conventional ellipsometry for a number of functionally important semiconductors, including the recently emergent organic non-fullerene electron acceptors (NFAs) and perovskites for which the optical constants in the UV–vis–near IR region are provided. Notably, the NFAs are found to present anomalously high refractive indices and extinction coefficients that are predicted to have a profound influence on the cavity electro-optics of the new record efficiency organic solar cells of which they are key components.

1. Introduction

Accurate knowledge of the optical constants of thin film layers within an optoelectronic device is a vital requirement for performance modeling as well as for design optimization. These are central endeavors in the development of device platforms such as thin film solar cells,[1–4] light-emitting diodes,[6] waveguides,[7] photonic crystals,[8] and photodetectors.[9] Specifically, precise determination of refractive index and attenuation coefficient in combination with transfer matrix and drift diffusion models allows absorbed or emitted electromagnetic field distributions to be calculated as well as injected or photogenerated charge profiles as a function of wavelength, stack structure, nano-morphology, composition, etc. to be determined.[1–4]

Despite being somewhat resource-intensive, spectroscopic ellipsometry is the most advanced and well-known technique for the determination of optical constants of thin film materials. Ellipsometry is relatively straightforward for thin films that are weakly absorbing and/or do not scatter. However, for poly- and semi-crystalline solids such as organic dyes and perovskites, which may be highly dispersive, non-isotropic, and present bulk or surface scattering, ellipsometry is very challenging and often inaccurate. This is due to several issues, but notably the fact that ellipsometry is intrinsically a polarization technique in which two fitted variables, φ and δ, must be determined from the ratio of the s- and p-polarized reflected light (ρ)

$$\rho = \frac{r_p}{r_s} = \tan(\varphi)\cdot e^{-i\delta} \tag{1}$$

where $\tan(\varphi)$ is the ratio of the s- and p-polarized field amplitudes and δ is the corresponding ratio of the phases. This fitting is initially performed in the so-called Cauchy regime (the sub-bandgap region where absorption is negligible) to estimate the film physical thickness. The fitting is then expanded to energies above the band gap using either a B-spline or general oscillator model (see the work of Tompkins et al. for a standard description of this method[10]). However, in the presence of anisotropy and/or scattering, this modeling is more difficult to perform, and it becomes even more challenging for strongly absorbing materials such as most perovskites and some organic semiconductor blends used in high-efficiency organic solar cells. Recent advanced ellipsometric hardware and software have made such analyses and modeling more tractable, but they are still time

R. Kerremans, C. Kaiser, Dr. W. Li, N. Zarrabi, Prof. P. Meredith, Dr. A. Armin
Sustainable Advanced Materials Programme (Sêr-SAM)
Department of Physics
Swansea University
Singleton Park, Swansea, Wales SA2 8PP, UK
E-mail: paul.meredith@swansea.ac.uk; ardalan.armin@swansea.ac.uk

The ORCID identification number(s) for the author(s) of this article can be found under https://doi.org/10.1002/adom.202000319.

DOI: 10.1002/adom.202000319

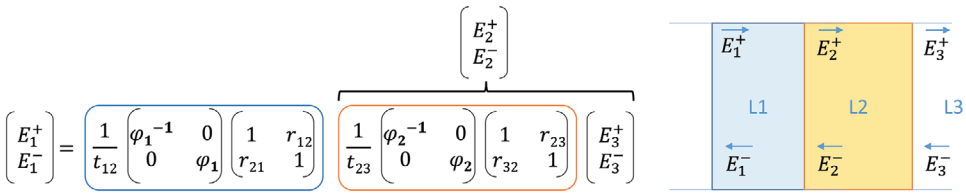

Figure 1. The standard transfer matrix method. The electric field is treated as a vector consisting of the forwards- and backwards-propagating components of the field. φ is a phase factor depending on the layer thickness, while t_{ij} and r_{ij} are the Fresnel coefficients, depending on the layers' (effective) optical constants.

and resource intensive and prone to considerable error (an oft-ignored fact). Therefore, there remains a strong motivation to develop complementary and, if possible, more simplistic and less resource-intensive approaches to determining the optical constants of thin film solids, especially with the rising popularity and increasing utility of organic semiconductors[11,5] and organohalide perovskites.[12,16]

In this current work, we introduce a method that can determine layer thicknesses and optical constants from the transmittance spectra of two thin film samples of the same material with different thicknesses in combination with an inverse transfer matrix approach.[1–4,13] The transfer matrix is entirely dependent on the thicknesses and optical constants of the layers within any arbitrary film stack (see **Figure 1**), and starting from this knowledge, it can describe the total transmittance and distribution of the electromagnetic field within a single or multiple layers.[13,14] Our methodology implements a reverse matrix approach to obtain layer thicknesses and optical constants, starting from transmittance data. A similar methodology has been reviewed previously,[15] but has not yet been examined experimentally and especially not for solution-processed semiconductors. Moreover, we employ only transmittance data, which is a distinct advantage over combined reflectance–transmittance strategies.[15] Our work was particularly motivated by a need to thoroughly investigate and model the record efficiency non-fullerene acceptor organic solar cell materials, which appear to have quite different electro-optical physics to more standard n-and-p-type organic semiconductors. It also transpires that the method is particularly suited to determining the optical constants of the organohalide perovskites. As a validation of the new approach, we compare the results with those obtained by spectroscopic ellipsometry for various materials and derive an optical external quantum efficiency (EQE) model for a set of standard solar cell devices, which is also compared to the experimental EQE data as the ultimate confirmation.

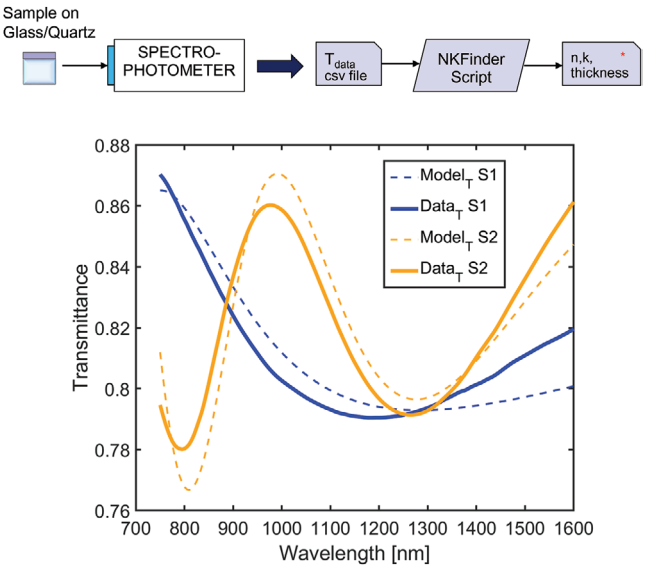

Figure 2. Top: A general overview of the transmittance/transfer matrix procedure when modeling a single-layer or multilayer stack with unknown optical constants. Once the optical constants have been derived, the device model can be used to model useful properties such as EQE. Bottom: Example of the fit quality obtained from the Cauchy regime fitting procedure in a direct analogy with the first stage of fitting in ellipsometry.

2. Theoretical Outline of the Transmittance Method

A schematic overview of the full transmittance method is given in **Figure 2** and in the flowchart of Figure S3, Supporting Information, and will now be discussed in more detail. A MATLAB computer code (denoted NKFinder) was developed for performing the calculations and can be found in the Supporting Information as freeware.

2.1. Cauchy Regime

First, the Cauchy regime of the transmittance spectrum of an absorbing thin film is defined as the above band gap spectral range where the imaginary component of the refractive index (the attenuation coefficient) k is approximately zero. This can be identified by determining the absorption onset from a sudden drop in the transmittance. The film thickness and real part of the refractive index (n) are the only required unknowns to fully model the film in this regime. In the Cauchy model, n can be approximated by $n = n_{\text{cauchy}} + B_{\text{cauchy}}/\lambda^2$ (where λ is the wavelength and B_{cauchy} is a proportionality factor), in other words by a second-order Cauchy approximation.[15] By performing a global fit across the Cauchy regime for two samples of the same material but different thickness, we can specify a range for the thicknesses of both samples and for one shared n value. The implicit assumption in this approach is that the film optical constants are approximately thickness independent. Once an appropriate fit is reached, the simulated transmittance is compared with the experimental values (see Figure 2) in a primary evaluation step. During this initial fitting, a scattering (baseline correction) parameter is also derived, which constitutes the

average difference in value between the experimental curve and the fitted curve. As such, any spectrally independent noise is filtered out and the fit relies only on the spectral curve shape (i.e., the thickness-dependent fringes in the Cauchy regime).

2.2. Full Spectral Range

After obtaining the sample thicknesses and refractive index within the Cauchy regime, the complex refractive index $\overline{n} = n + ik$ can be calculated across the full spectrum. We can again use the transfer matrix method to calculate transmittance, this time for a varying attenuation coefficient k. For the first iteration, we assume that the real part of the complex refractive index n equals the previously found $n_{\text{cauchy}} + B_{\text{cauchy}}/\lambda_{\text{cauchy}}^2$ across the full spectrum. This approach will already give a good estimate, because the transmittance of highly absorbing thin films is much less sensitive to the real component n than to the imaginary part k. This becomes obvious when considering that transmittance T depends on reflectance R and absorptance A via

$$T + R + A = 1 \tag{2}$$

where R changes slowly with the difference in $\overline{n}$ of each medium

$$R = \left|r_{\text{Fresnel}}\right|^2 = \left|\frac{\overline{n}_1 - \overline{n}_2}{\overline{n}_1 + \overline{n}_2}\right|^2 \tag{3}$$

and A exponentially with the imaginary component k[1,23]

$$A = \int_0^t \alpha(x) I(x) dx \tag{4}$$

$$A = \int_0^t \frac{4\pi k(x)}{\lambda} \cdot \frac{c\varepsilon_0 n}{2} E_M^2 e^{\frac{-4\pi k x}{\lambda}} dx \tag{5}$$

Here $\alpha(x)$ is the absorption coefficient and $I(x)$ is the light intensity proportional to the squared norm of the electric field, $|E(x)|^2$. After we have an initial estimate of the imaginary component k across the full spectrum, we can use the Kramers–Kronig relations to derive a new, improved estimate of n. The Kramers–Kronig relations are commonly presented in their form for the dielectric constants, but are also valid for the optical constants as shown by Bohren.[17] The real part of the complex index, n, can be presented as a function of radial frequency ω

$$n(\omega) = 1 + \frac{2}{\pi} \oint_0^\infty \frac{\omega' \cdot k(\omega')}{\omega'^2 - \omega^2} d\omega' \tag{6}$$

as well as a function of wavelength, λ, which can be more intuitive when working with spectral transmittance

$$n(\lambda) = 1 + 4c \oint_0^\infty \frac{\frac{2\pi c}{(\lambda')^3} \cdot k(\lambda')}{\left(\frac{2\pi c}{\lambda'}\right)^2 - \left(\frac{2\pi c}{\lambda}\right)^2} d\lambda' \tag{7}$$

Because this integral runs from zero to infinity, certain assumptions must be accommodated when calculating $n(\lambda)$. In the Cauchy regime, $k(\lambda)$ will be approximately zero and therefore the contribution of this integral above the band gap cut-off can be neglected. However, an estimate for $k(\lambda \to 0)$ (above gap and towards the high-energy UV regime) has to be made since standard spectrophotometers of the sort used to obtain transmittance measurements are usually limited to ≈300 nm at the lower end of their range. This estimate can be achieved by assuming a simple band model for the semiconductor based on the Tauc model[18,24]

$$\left(\alpha_{ij} h\nu\right)^{1/m} = A_{ij}\left(h\nu - E_{g,ij}\right) \tag{8}$$

where $m = 1/2$ for direct allowed transitions and $m = 2$ for indirect allowed transitions. A is a proportionality constant that can be determined experimentally, and ij denote the examined band structures. Usually, in the visible spectrum, there are only two relevant bands—the valence and conduction. But as we approach shorter wavelengths (or photons of higher energy), deeper valence bands in the material also become accessible for charge carrier light absorption.[14] As a consequence, the total absorption coefficient at high energies is the sum over the band absorption coefficients α_{ij}[21]

$$\alpha_{\text{total}}(\lambda) = \frac{4\pi k(\lambda)}{\lambda} = \sum\nolimits_{ij} \alpha_{ij}(\lambda) \tag{9}$$

By implementing a qualitative model derived from this simple formula, we can add an extra band structure towards $\lambda = 0$, using similar proportionality values to the A found in the visible spectrum for the primary band transition. This is a very simplistic approximation, but the exact shape of $k(\lambda)$ in this lower wavelength regime turns out to have a minor effect on $n(\lambda)$ in the visible spectral range (see Figure S2, Supporting Information). We note that because of this approximation, there will be higher uncertainty in $\overline{n}(\lambda)$ deep in the UV.

Using these assumptions, we arrive at a satisfactory relation between n and k. It is also possible to make the method recursive, by reusing the as-derived n to find a more accurate extinction coefficient k. However due to the strong relation between k and the transmittance as indicated above, such a recursion often converges on the first iteration. The flowchart of Figure S3, Supporting Information, illustrates the full process.

3. Results and Discussion

The transmittance methodology was first tested on simulated transmittance data, calculated from known input optical constants. The results of this input-output test can be found in Figure S1, Supporting Information, and show a near-identical output, which is only inexact because the input optical constants are ellipsometric and not derived from a Kramers–Kronig relation. The transfer matrix code was also validated against the commercially available electro-optics software SETFOS.[19] Once these verification steps were completed, the method was applied to a number of different thin films on glass (each material or material blend of two thicknesses) and spectroscopic ellipsometry was also performed on the same films. The samples were as follows (full chemical definitions can be found in the Experimental Section): 1) $PC_{71}BM$; 2) PCDTBT; 3) 1:4 PCDTBT:$PC_{71}BM$ blend; 4) 1:4 PCPDTBT:$PC_{71}BM$ blend; 5) 1:1 P3HT:$PC_{61}BM$ blend; 6) 1:1.5 PTB7-Th:$PC_{71}BM$ blend; 7) 1:1 PBDB-T:ITIC blend; 8) 1:1 PTB7-Th:ITIC blend; 9) 1:1 PBDB-T:IT-4F blend; 10) PM6; 11) Y6; 12) 1:1.2 PM6:Y6 blend;

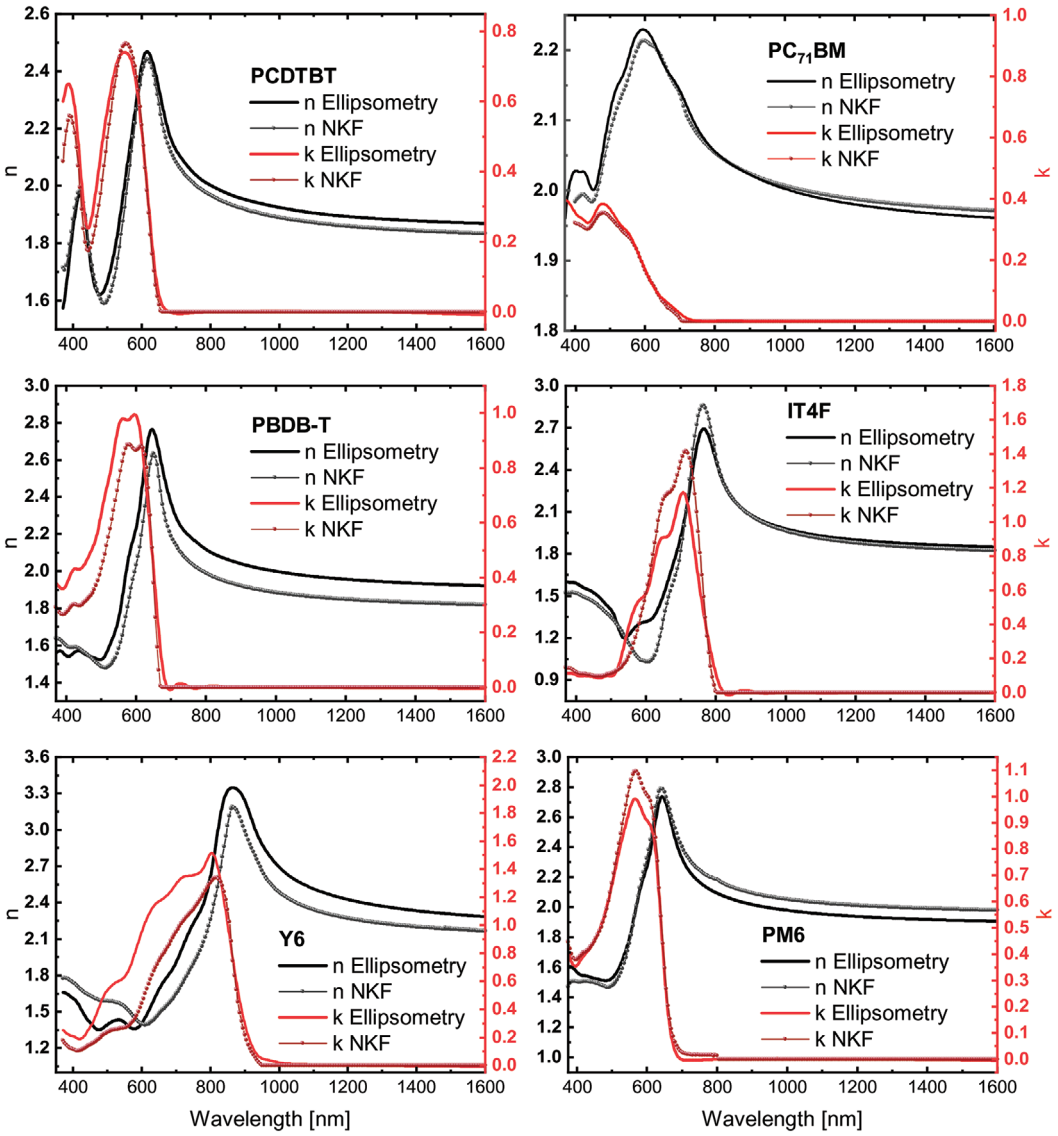

Figure 3. Comparison of n-and-p-type organic semiconductors (neat materials) optical constants derived by ellipsometry (solid lines) and via the transmittance method (dotted lines). The refractive index (n) and attenuation coefficients (k) are represented on the left and right y-axis, respectively. We note the non-fullerene acceptors Y6 and IT-4F have significantly larger optical constants than their fullerene counterpart $PC_{71}BM$.

13) 1:1 PM6:IT-4F blend; and 14) $MAPbI_2Br$ mixed halide perovskite. This portfolio of thin films represents a very robust test of the transmittance methodology and contains archetypal organic semiconductor fullerene-based acceptor: donor blends and some of the highest reported efficiency non-fullerene organic solar cell materials.

The optical constant results for several of these neat semiconductor and blend films are shown in **Figure 3** for the neat materials and in **Figure 4** for the blends, where they are compared with the corresponding ellipsometry analyses. The remaining material results are provided in the Supporting Information. As can be seen in these figures, the two methods deliver comparable optical constants with some deviations for $n(\lambda)$ at shorter wavelengths (<400 nm), which are mainly due to the extension of $k(\lambda)$ in the Kramers–Kronig procedure. This is also complicated by the substrate (glass or quartz) absorption below the band edge. For non-fullerenes and perovskites, the deviation is larger due to their high optical constants and higher degree of anisotropy, which complicates the ellipsometric measurements and fittings.

There are a number of interesting features of the transmittance method results. First, in the case of the non-fullerenes, the optical constants were successfully derived even in the lower wavelength range, where the ellipsometric method tends to fail due to the high optical constants involved. This is, for example, the case for ITIC and IT-4F based blends (see Figure 4), where the ellipsometry fitting in the absorbing regime has relatively high mean square error values, while the transmittance method gives consistent results for both the ITIC and IT-4F. We note that ITIC and IT-4F are very similar chemically and should therefore have similar optical constants. Their absorption coefficients were published previously

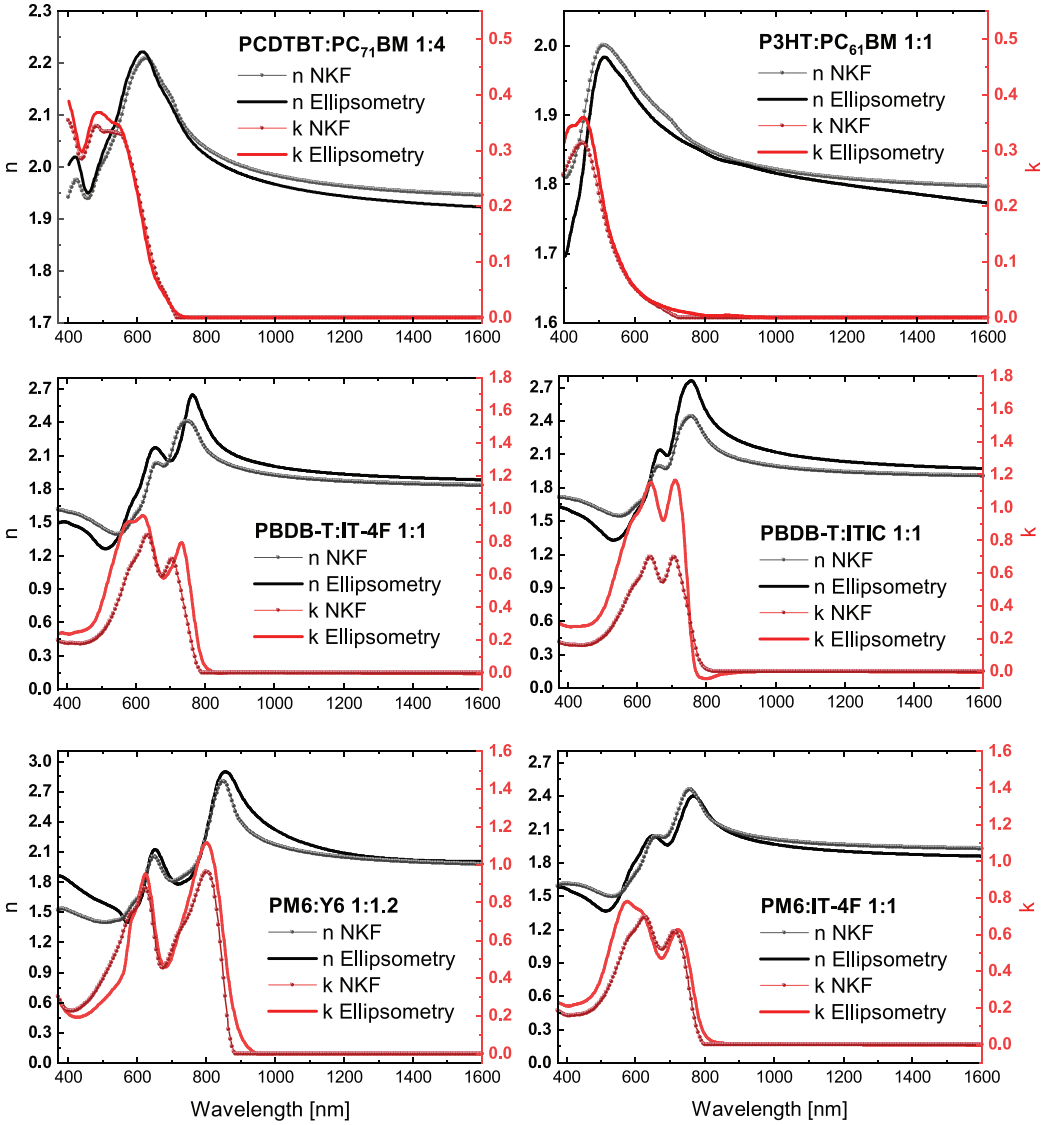

Figure 4. Comparison of n-and-p-type organic semiconductors (acceptor-donor blends) optical constants derived by ellipsometry (solid lines) and via the transmittance method (dotted lines). The refractive indices (*n*) and attenuation coefficients (*k*) are represented on the left and right *y*-axis, respectively. We note the high optical constants seen in the neat NFAs are translated through to the blends.

by independent authors,[20] and match the constants derived with the transmittance method quite well. Second, we observe another particular challenge with some non-fullerenes—an apparent thickness dependence of the optical constants as different optical constants are obtained from samples with different thickness (see Figure S9, Supporting Information). We believe this to be derived from a thickness dependence of the morphology and crystallinity. Third, both neat films and blends of the NFAs possess anomalously high optical constants relative to their more traditional n-and-p-type equivalents. For example, the record efficiency NFA Y6 possesses a peak refractive index of ≈3.3 while the equivalent fullerene $PC_{71}BM$ peaks at ≈2.2. The attenuation coefficients are likewise unexpectedly large (>1.0) for the NFAs and these features project through into the blends. The observations have potentially significant implications for the electro-optical cavity effects in thin film structures such as solar cells, and one could also speculate as to the role of these anomalously high optical constants in delivering very efficient solar energy harvesting. Finally, we note that the organohalide perovskites pose the same challenges for standard ellipsometry,[2] and successful transmittance-derived constants for a mixed halide perovskite are presented in the Supporting Information to demonstrate the applicability of the method to this second class of important solution processed semiconductors.

To complete the validation of the transmittance method, full device EQEs were determined experimentally and simulated from the derived optical constants. This was performed on several solar cell devices fabricated using 1:4 blend ratio PCDTBT:$PC_{71}BM$ with varying active layer thicknesses. These devices were then simulated using the optical constants derived with the transmittance method, to model

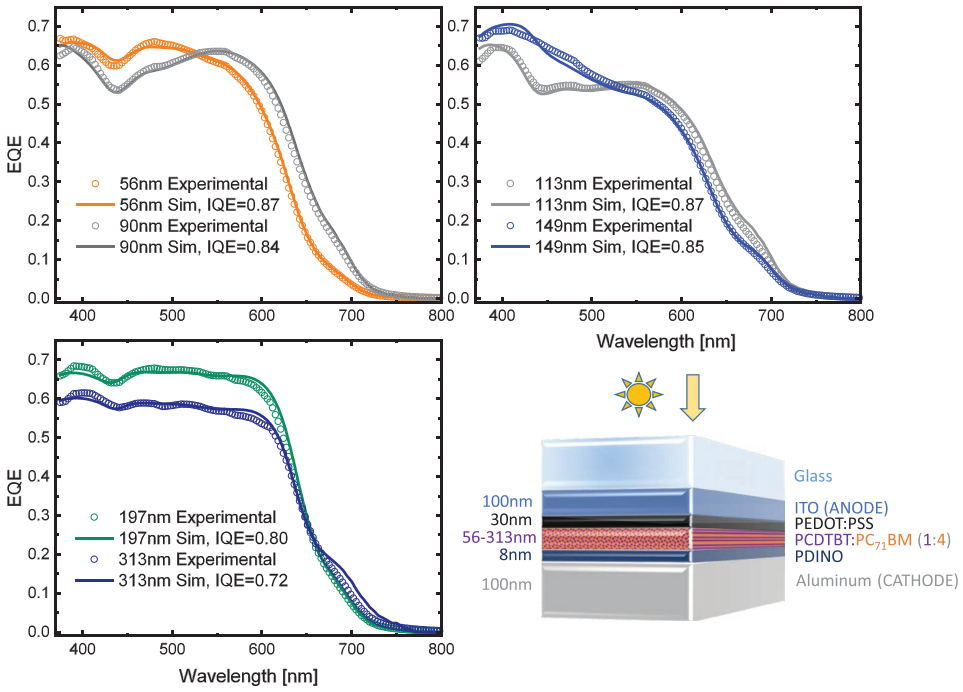

Figure 5. Solar cell experimental and modeled EQEs for devices containing a PCDTBT:$PC_{71}BM$ active layer (different thicknesses and structure shown in the schematic). The transmittance-derived optical constants were used to compute each respective solar cell EQE and find a subsequent spectrally constant fit for the IQE. As one would predict the IQE of the thicker junction is lower due to non-optimal charge collection indicative of PCDTBT:$PC_{71}BM$.

each devices' ideal EQE. **Figure 5** shows a comparison of the experimental EQE data with the modeled EQEs fitted using a spectrally constant internal quantum efficiency (IQE), which is given in the plot legends. A spectrally constant IQE is predicted by previous measurements[3,21] and validated in Figure S10, Supporting Information. We first observe that the modeled IQE increases with decreasing active layer thickness as expected from drift-diffusion models. Second, and most importantly, the spectral shape of the EQE and derived IQE is reproduced in the modeled spectra, indicating accurate optical constants. This approach could also be applied to non-fullerene-based solar cells, although it is by no means clear that these IQEs are spectrally flat and we continue work along these lines.

Finally, it is also worthy of note that the transmittance methodology described above enables a simple alternative for the modeling of complex anisotropic, porous, or blended layers as an effective single layer. It does not require any computation of underlying concentration parameters, anisotropy, or effective optical constants along the lines of Bruggeman or Maxwell-Garnett models[22] as for the fitting of ellipsometric data, which cannot always accurately model blends as a single layer. The method can also be applied to purely transparent layers, or to determine low absorption coefficients by using relatively thicker samples. Furthermore, the implemented transfer matrix formalism, which is based on the work of Harbecke,[13] also incorporates the possibility of angular-dependent reflectance, which could be a valuable extension for particularly complex composite films. Hence, we would contend that the utility of the method has very significant potential for extension.

4. Conclusion

In conclusion, we report a new transmittance-based methodology to determine the optical constants of thin films that is particularly suited to solution-processed, next-generation semiconductors such as organics and organohalide perovskites. The approach relies upon an inverse transfer matrix formalism with Kramers–Kronig reconstruction on films of two thicknesses. We have applied the method to a range of n-and-p-type organic semiconductors and a mixed halide perovskite. The determined optical constants agree well with the more resource intensive ellipsometry when the latter technique is able to provide a reliable solution. We also validate the results by modeling and measuring full solar cell EQEs and find excellent agreement. The method has been used to determine the optical constants of several non-fullerene acceptor materials that are the basis for new record efficiency organic solar cells. We find anomalously high refractive indices and attenuation coefficients in these systems with an identifiable thickness dependence. This highlights the very different electro-optical physics of the NFAs and maybe is a pointer towards understanding why they are first so difficult to model and second, deliver such high power conversion efficiencies.

5. Experimental Section

Chemical Definitions: $PC_{71}BM$: [6,6]-phenyl-C_{71}-butyric acid methyl ester; PCDTBT: poly[N-9′-heptadecanyl-2,7-carbazole-alt-5,5-(4′,7′-di-2-thienyl-2′,1′,3′-benzothiadiazole)]; PCPDTBT: poly[2,6-(4,4-bis-(2-ethylhexyl)-4*H*-cyclopenta [2,1-b;3,4-*b*′]dithiophene)-*alt*-4,7(2,1,3-benzothiadiazole)]; P3HT: poly(3-hexylthiophene-2,5-diyl); $PC_{61}BM$: [6,6]-phenyl-C61-butyric acid methyl ester; PTB7-Th: poly[4,8-bis(5-(2-ethylhexyl)

thiophen-2-yl)benzo[1,2-b;4,5-*b′*]dithiophene-2,6-diyl-*alt*-(4-(2-ethylhexyl)-3-fluorothieno[3,4-*b*]thiophene-)-2-carboxylate-2-6-diyl)]; PBDB-T: poly[(2,6-(4,8-bis(5-(2-ethylhexyl)thiophen-2-yl)-benzo[1,2-*b*:4,5-*b′*]dithiophene))-*alt*-(5,5-(1′,3′-di-2-thienyl-5′,7′-bis(2-ethylhexyl)benzo[1′,2′-*c*:4′,5′-*c′*]dithiophene-4,8-dione)]; ITIC: 3,9-bis(2-methylene-(3-(1,1-dicyanomethylene)-indanone))-5,5,11,11-tetrakis(4-hexylphenyl)-dithieno[2,3-*d*:2′,3′-*d′*]-*s*-indaceno[1,2-*b*:5,6-*b′*]dithiophene; IT-4F: 3,9-bis(2-methylene-((3-(1,1-dicyanomethylene)-6,7-difluoro)-indanone))-5,5,11,11-tetrakis(4-hexylphenyl)-dithieno[2,3-*d*:2′,3′-*d′*]-*s*-indaceno[1,2-b:5,6-*b′*]dithiophene; PM6: poly[(2,6-(4,8-bis(5-(2-ethylhexyl-3-fluoro)thiophen-2-yl)-benzo[1,2-*b*:4,5-*b′*]dithiophene))-*alt*-(5,5-(1′,3′-di-2-thienyl-5′,7′-bis(2-ethylhexyl)benzo[1′,2′-*c*:4′,5′-*c′*]dithiophene-4,8-dione)]; Y6: 2,2′-((2*Z*,2′*Z*)-((12,13-bis(2-ethylhexyl)-3,9-diundecyl-12,13-dihydro-[1,2,5]thiadiazolo[3,4-e]thieno[2′′,3′′:4′,5′]thieno[2′,3′:4,5]pyrrolo[3,2-*g*]thieno[2′,3′:4,5]thieno[3,2-*b*]indole-2,10-diyl)bis(methanylylidene))bis(5,6-difluoro-3-oxo-2,3-dihydro-1*H*-indene-2,1-diylidene))dimalononitrile; MAPbI2Br: methylammonium lead iodide bromide; PDINO: 2,9-bis[3-(dimethyloxidoamino)propyl]anthra[2,1,9-def:6,5,10-*d′e′f′*]diisoquinoline-1,3,8,10(2*H*,9*H*)-tetrone.

Film Preparation: $PC_{71}BM$, P3HT, and PbI_2 were purchased from Merck. PCDTBT, PCPDTBT, chlorobenzene (CB), chloroform (CF), 1,2-dichlorobenzene (DCB), 1,8-diiodooctane (DIO), and 1-chloronaphthalene (CN) were purchased from Sigma-Aldrich. PTB7-Th, PBDB-T, ITIC, PM6, Y6, and IT-4F were purchased from Nanjing Zhiyan, Inc. MABr was purchased from Dyesol. All materials were used as received without further purification. The thin films were fabricated by spin-coating the relevant solutions on 2.5 × 2.5 cm glass substrates in an inert environment in glovebox using the solvents and concentration given in the following paragraph.

$PC_{71}BM$ was dissolved in CB at a concentration of 20 mg mL^{-1} and spin-coated on glass at 1000 rpm and 800 rpm. PCDTBT was dissolved in DCB at a concentration of 3 mg mL^{-1} at 100 °C. Once the PCDTBT was fully dissolved, the solution was left to cool to room temperature and spin-coated on glass at 1500 rpm. 1:4 PCDTBT:$PC_{71}BM$: PCDTBT and $PC_{71}BM$ were dissolved in DCB with the donor/acceptor ratio of 1:4, and the thickness of active layers was adjusted by changing the concentration of the solution and the speed of spin-coating (30 mg mL^{-1} DCB solution with 1500 rpm for 54 nm active layer, 40 mg mL^{-1} DCB solution with 1500 rpm for 85 nm active layer, 40 mg mL^{-1} DCB solution with 1000 rpm for 105 nm active layer, 40 mg mL^{-1} DCB solution with 600 rpm for 155 nm active layer, 50 mg mL^{-1} DCB solution with 600 rpm for 185 nm active layer, 60 mg mL^{-1} DCB solution with 600 rpm for 315 nm active layer, and 60 mg mL^{-1} DCB solution with 400 rpm for 585 nm active layer). 1:4 PCPDTBT:$PC_{71}BM$: PCPDTBT and $PC_{71}BM$ (with a ratio of 1:4) were dissolved in a CB/DCB (1:1) mixture solution at 70 °C at the concentration of 40 mg mL^{-1} followed by cast on glass substrates. 1:1 P3HT:$PC_{61}BM$: P3HT and $PC_{61}BM$ (with a ratio of 1:1) were dissolved in DCB at 70 °C at the concentration of 30 mg mL^{-1}. Then it was cast on glass substrates at 600 rpm followed by thermal annealing at 150 °C for 30 min. 1:1.5 PTB7-Th:$PC_{71}BM$: PTB7-Th and $PC_{71}BM$ (with the ratio of 1:1.5) were dissolved in CB (with 3% DIO) at 60 °C at a concentration of 14 mg mL^{-1} and spin-coated on glass substrates. Then the as-cast films were rinsed with 80 µL methanol at 4000 rpm for 20 s to remove the residual DIO. 1:1 PBDB-T:ITIC: PBDB-T and ITIC (with the ratio of 1:1) were dissolved in CB (with 0.5% DIO) at a concentration of 14 mg mL^{-1}, and then it was spin-coated on glass substrates at 1000 rpm followed by thermal annealing at 100 °C for 10 min. 1:1 PTB7-Th:ITIC: PTB7-Th and ITIC (with a ratio of 1:1) were dissolved in CB (with 1% DIO) at 60 °C at a concentration of 14 mg mL^{-1}, and then it was spin-coated on glass substrates at 1000 rpm. 1:1 PBDB-T:IT-4F: PBDB-T and IT-4F (with the ratio of 1:1) were dissolved in CB (with 0.5% DIO) at a concentration of 14 mg mL^{-1}, and then it was spin-coated on glass substrates at 1000 rpm followed by thermal annealing at 100 °C for 10 min. PM6 was dissolved in CF at a concentration of 14 mg mL^{-1} and spin-coated on glass substrates at 2500 rpm. Y6 was dissolved in CF at a concentration of 25 mg mL^{-1} and spin-coated on glass substrates at 2500 rpm. 1:1.2 PM6:Y6: PM6 and Y6 (with the ratio of 1:1.2) were dissolved in CF (with 0.5% CN) at a concentration of 16 mg mL^{-1}, and then it was spin-coated on glass substrates at 3000 rpm followed by thermal annealing at 110 °C for 10 min. 1:1 PM6:IT-4F: PM6 and IT-4F (with the ratio of 1:1) were dissolved in CF (with 0.5% CN) at a concentration of 16 mg mL^{-1}, and then it was spin-coated on glass substrates at 3000 rpm followed by thermal annealing at 110 °C for 10 min. $MAPbI_2Br$ mixed halide perovskite: PbI_2 and MABr were dissolved according to 1:1 molar ratios in a solvent mixture of 4:1 DMF:DMSO under a concentration of 804 mg mL^{-1}. The solution was heated to 60 °C for 1 h and subsequently spin-coated on a glass substrate at 4000 rpm, dropping ethyl acetate as the anti-solvent for 10 s during the spin coating. After this, the substrates were annealed at 100 °C for 1 h and immediately analyzed to prevent any severe atmospheric deterioration.

Device Fabrication: PCDTBT:$PC_{71}BM$ devices were fabricated with a so-called conventional bulk heterojunction architecture (ITO/PEDOT:PSS/PCDTBT:$PC_{71}BM$/PDINO/Al). Commercial patterned ITO-coated glass substrates (Ossila) were cleaned in an Alconox (detergent) solution bath at 60 °C, followed by sonication in sequence in deionized water, acetone, and 2-propanol for 10 min each. After treatment with UV-ozone (L2002A2-UK, Ossila) for 10 min, 30 nm of PEDOT:PSS was spin-coated on the clean ITO substrates. Then PCDTBT:$PC_{71}BM$ films with different thicknesses were spin-coated on PEDOT:PSS (as described above). Afterwards, 10 nm of PDINO was cast on active layer from methanol solution (1 mg mL^{-1}), and then 100 nm of Al was evaporated on PDINO to form the cathode.

Supporting Information

Supporting Information is available from the Wiley Online Library or from the author.

Acknowledgements

This work was funded by the Welsh Government's Sêr Cymru II Program (Sustainable Advanced Materials) through the European Regional Development Fund and Welsh European Funding Office. R.K. and C.K. are the recipients of EPSRC DTP postgraduate awards. P.M. is a Sêr Cymru II Research Chair and A.A. a Sêr Cymru II Rising Star Fellow.

Conflict of Interest

The authors declare no conflict of interest.

Keywords

external quantum efficiency, non-fullerene acceptors, optical constants, perovskites, solar cells

Received: February 24, 2020
Revised: April 8, 2020
Published online:

[1] L. A. A. Pettersson, L. S. Roman, O. Inganäs, *J. Appl. Phys.* **1999**, *86*, 487.
[2] Q. Lin, A. Armin, R. C. R. Nagiri, P. L. Burn, P. Meredith, *Nat. Photonics* **2015**, *9*, 106.
[3] A. Armin, M. Velusamy, P. Wolfer, Y. Zhang, P. L. Burn, P. Meredith, A. Pivrikas, *ACS Photonics* **2014**, *1*, 173.
[4] R. Kerremans, O. J. Sandberg, S. Meroni, T. Watson, A. Armin, P. Meredith, *Sol. RRL* **2020**, *4*, 1900221.

[5] C. Yan, S. Barlow, Z. Wang, H. Yan, A. K.-Y. Jen, S. R. Marder, X. Zhan, *Nat. Rev. Mater.* **2018**, *3*, 18003.
[6] Z. Liu, K. Wang, X. Luo, S. Liu, *Opt. Express* **2010**, *18*, 9398.
[7] G. Stewart, B. Culshaw, *Opt. Quantum Electron.* **1994**, *26*, S249.
[8] A. Lavrinenko, P. I. Borel, L. H. Frandsen, M. Thorhauge, A. Harpøth, M. Kristensen, T. Niemi, H. Chong, *Opt. Express* **2004**, *12*, 234.
[9] K. H. An, B. O'Connor, K. P. Pipe, M. Shtein, *Org. Electron.* **2009**, *10*, 1152.
[10] H. G. Tompkins, J. Hilfiker, *Spectroscopic Ellipsometry, Practical Application to Thin Film Characterization*, Momentum Press, New York **2016**.
[11] S. K. Hau, H.-L. Yip, A. K.-Y. Jen, *Polym. Rev.* **2010**, *50*, 474.
[12] Z. Song, S. C. Watthage, A. B. Phillips, M. J. Heben, *J. Photonics Energy* **2016**, *6*, 022001.
[13] B. Harbecke, *Appl. Phys. B: Photophys. Laser Chem.* **1986**, *39*, 165.
[14] L. A. Pettersson, L. S. Roman, O. Inganäs, *J. Appl. Phys.* **1999**, *86*, 487.
[15] D. Poelman, P. F. Smet, *J. Phys. D: Appl. Phys.* **2003**, *36*, 1850.
[16] Y. Bai, S. Xiao, C. Hu, T. Zhang, X. Meng, H. Lin, Y. Yang, S. Yang, *Adv. Energy Mater.* **2017**, *7*, 1701038.
[17] C. F. Bohren, *Eur. J. Phys.* **2010**, *31*, 573.
[18] B. D. Viezbicke, S. Patel, B. E. Davis, D. P. Birnie III, *Phys. Status Solidi B* **2015**, *252*, 1700.
[19] FLUXiM AG, *Semiconducting emissive thin film optics simulator, SETFOS* **2018**, https://www.fluxim.com/setfos-intro (accessed: May 2020).
[20] W. Zhao, S. Li, H. Yao, S. Zhang, Y. Zhang, B. Yang, J. Hou, *J. Am. Chem. Soc.* **2017**, *139*, 7148.
[21] S. H. Park, A. Roy, S. Beaupre, S. Cho, N. Coates, J. S. Moon, D. Moses, M. Leclerc, K. Lee, A. J. Heeger, *Nat. Photonics* **2009**, *3*, 297.
[22] D. Aspnes, *Am. J. Phys.* **1982**, *50*, 704.
[23] O. S. Heavens, *Optical Properties of Thin Films*, Courier Corporation, Chelmsford, MA **1991**.
[24] J. Tauc, R. Grigorovici, A. Vancu, *Phys. Status Solidi B* **1966**, *15*, 627.